Mediterranean Overflow Water (MOW) simulation using a coupled multiple-grid Mediterranean Sea/North Atlantic Ocean model

David E. Dietrich,[1] Yu-Heng Tseng,[2] Raul Medina,[3] Steve A. Piacsek,[4] Maria Liste,[3] Maitane Olabarrieta,[3] Malcolm J. Bowman,[5] and Avichal Mehra[6]

Received 31 January 2007; revised 12 January 2008; accepted 28 February 2008; published 22 July 2008.

[1] A z-level, 4th-order-accurate ocean model is applied in six two-way-coupled grids spanning the Mediterranean Sea and North Atlantic Ocean (MEDiNA). Resolutions vary from 1/4° in central North Atlantic to 1/24° in Strait of Gibraltar region. This allows the MEDiNA model to efficiently resolve small features (e.g., Strait of Gibraltar) in a multibasin, multiscale model. Such small features affect all scales because of nonlinearity and low dissipation. The grid coupling using one coarse grid overlap is nearly seamless without intergrid sponge layers. No instant convective adjustment or other highly diffusive process is used. The deep water in the 1/8° Mediterranean Sea grid is formed by the resolved flows that emulate subgrid-scale processes directly. Downslope migration of Mediterranean Overflow Water (MOW) water involves dense water flowing away from the bottom laterally over bottom stairsteps in the z-level model, thus flowing over less dense underlying water. Without excessively water mass-diluting process, the advection dominates the downslope migration of thin, dense MOW in the simulation. The model results show realistic MOW migration to the observed equilibrium depth, followed by lateral spreading near that depth. The results are also consistent with the climatology along 43°N, where the MOW hugs a steep shelfslope centered at ~1 km depth and then spreads westward, with the salinity core (S > 35.7) reaching 18°W. This study clearly restores z-level models to a competitive status doing density current simulations.

Citation: Dietrich, D. E., Y.-H. Tseng, R. Medina, S. A. Piacsek, M. Liste, M. Olabarrieta, M. J. Bowman, and A. Mehra (2008), Mediterranean Overflow Water (MOW) simulation using a coupled multiple-grid Mediterranean Sea/North Atlantic Ocean model, *J. Geophys. Res.*, *113*, C07027, doi:10.1029/2006JC003914.

1. Introduction

1.1. Background

[2] Modeling the downslope penetration of density currents spilling over sills is of considerable research interest and important [e.g., *Peters et al.*, 2005; *Legg et al.*, 2005; *Killworth*, 2001; *Killworth and Edwards*, 1999]. *Dietrich et al.* [2004a], using a purely z-level model, showed that only when the New England shelfslope density current is sufficiently intense and undiluted to reach the Cape Hatteras abutment does the Gulf Stream separate there and pinch off warm- and cold-core rings similar to those observed. Strong inertial flow (high Reynolds number based on the scale of the abutment) is necessary but not sufficient. Separation occurs there only if the model resolution is fine enough or the model dissipation and numerical dispersion are sufficiently small to avoid dilution and loss of intensity during its long transit time from its high latitude seas sources. The thinness and narrowness of density currents makes them difficult to resolve and accurately model.

[3] The main focus of this study is the dense Mediterranean Overflow Water (MOW), a thin, narrow intense current that spills over the Strait of Gibraltar sill. MOW is an even more model-challenging density current (see section 1.2) than the New England Shelfslope Current, the Red Sea outflow [*Peters et al.*, 2005] or the Denmark Strait Overflow [*Legg et al.*, 2005]. Although its properties change rapidly as it becomes diluted due to mixing and entrainment while flowing along the northern Gulf of Cadiz shelfslope, the MOW remains well defined as a deep, warm salty current between 1000 m and 1200 m depth all around the Atlantic coast of the Iberian Peninsula, and its deep water mass signature is seen over much of the central North Atlantic Ocean basin [*Curry et al.*, 2003]. *Ozkokmen et al.* [2001] have described a connection between the Mediterranean outflow and the Azores Current. Hence it is clear that the MOW is important in spite of its relatively small transport. It is dense because of its high salinity and is

[1] AcuSea, Inc., Via Sonoma, La Jolla, California, USA.
[2] Department of Atmospheric Sciences, National Taiwan University, Taipei, Taiwan.
[3] Ocean and Coastal Research Group, University of Cantabria, Santander, Spain.
[4] Oceanography Division, Naval Research Laboratory, Stennis Space Center, Mississippi, USA.
[5] Marine Sciences Research Center, State University of New York at Stony Brook, Stony Brook, New York, USA.
[6] Environmental Modeling Center, NCEP/NWS, NOAA, Camp Springs, Maryland, USA.

0148-0227/08/2006JC003914

much warmer than the ambient North Atlantic Central water (NACW) near the 300–400 m depth sill level [*Levitus and Boyer*, 1994]. Indeed, even after mixing with ambient NACW as it flows along the bottom slope of the Gulf of Cadiz, and after "sliding" toward deeper levels due to secondary flows induced by bottom friction, the MOW is about 5°C warmer than the far-field NACW at levels near the final equilibrium depth of about 1100 m. The MOW has significant climatological effects on the deep North Atlantic heat and salt balance.

[4] The contemporary MOW is saltier, warmer, denser and reaching deeper and further westward than it was in the last decades of the 20th century, before anthropogenic effects became evident [*Curry et al.*, 2003; *Rixen et al.*, 2005]. These include a combination of increased evaporation (greenhouse warming effect) and Aswan Dam diversion of ~90% of the Nile River to irrigation. The Mediterranean Sea mean salinity has increased by 0.04 during the last 40 years [*Bethoux et al.*, 1998; *Johnson*, 1997; TOPtoTOP Global Climate Expedition]. Mediterranean Sea ecosystems will eventually be affected by the salinity increase of the Mediterranean Seawater [*Millot*, 2007]. These potentially affect the currents, temperature, salinity and geobiochemical distributions and the associated ecosystem around the Iberian Peninsula and western Mediterranean Sea, and also the entire Mediterranean Sea [*Drillet et al.*, 2005]. The basin-scale thermohaline circulation involving water mass transformations in the Mediterranean Sea strongly affects this exchange. On the other hand, fresher and much less dense MAW (modified Atlantic Water) overrides the MOW through the Strait of Gibraltar and flows eastward into the Mediterranean Sea. It spreads quickly into a thin layer in the Alboran Sea and feeds an intense meandering current along the North Africa coast [*Tintore et al.*, 1988]. The MAW affects the entire Mediterranean Sea circulation; and is especially important in the Mediterranean coastal regions of the Iberian Peninsula. Sometimes, large MAW meanders even flow directly from the eastern Alboran Sea to as far north as the Balearic Islands and affect the surrounding water's physical and biogeochemical properties as far north as Mallorca [*Millot*, 1999, 2007]. This "inverse estuarine" or gravitational circulation tightly couples the Mediterranean Sea to the North Atlantic Ocean.

1.2. MOW Modeling Challenge

[5] Accurate modeling of the MOW is challenging because the MOW represents a very thin, bottom hugging, and dense (compared to the ambient MAW) current spilling into North Atlantic Ocean over a shallow sill in a narrow strait. It must be modeled without excessive water mass dilution, possibly caused by numerical dispersion errors (e.g., inaccurate numerical approximations), or by large numerical dissipation (required by some models for stability and numerical robustness). Accurate modeling of the sinking process also requires an accurate description of the source of this water, the thermohaline-forced exchange through the narrow Strait of Gibraltar, and the circulations in the two basins feeding the in- and outflows. Thus the significant modeling challenge is to realistically represent the vigorous exchange of NACW with MOW water through the Strait of Gibraltar, and the downslope penetration of its thin, narrow density current.

[6] *Johnson et al.* [2002] applied a 1/24° regional model to the southwestern Iberian Peninsula coastal region, west of the Strait of Gibraltar, and showed realistic MOW penetration including anticyclonic meddies at depth ~845 m (model level 16). In spite of the small scale and intensity of the bottom-hugging MOW, the entrainment of lighter ambient water was slow. The entrainment was limited by the large static stability at its top and insulated conditions (little heat or salt transfer) at the ocean bottom. Significant entrainment is possible only near its sloping baroclinic edge where baroclinic instability of eddies with small Rossby radius of deformation, *Ro*, occurs. The observations of its characteristic temperature and salinity signatures far from its source region indicate that this entrainment is slow especially after reaching its equilibrium level. Indeed, warm salty MOW water mass signatures are seen thousands of kilometers away from their source. Modeling such long-lasting current intensity and water mass conservation (far downstream from the MOW source) is impossible using models that require large viscosity/diffusion for numerical stability, and also difficult using models with large numerical dispersion.

[7] *Drillet et al.* [2005] recently applied a new version of the rigid-lid OPA model in an ultra-high resolution (~6 km and 43 z-levels) simulation of the coupled Mediterranean Sea and North Atlantic focusing on the MOW and the eddies ("meddies"). To overcome problems with the z-level grid, they introduced a relaxation scheme to climatology, applied within a radius encompassing the area of intense downflow in the Gulf of Cadiz region. The computational demands of a high resolution grid on such a large domain limit their simulation to only five model years, which is adequate to get near-equilibrium in the MOW dynamics in the southwest Iberian Peninsula region where meddies are spawned. They further relaxed their model toward climatology using spatially varying timescale, with the fastest (50 d) in the Cape St. Vincent region where meddies are formed. The modeled meddies properties, and the equilibrium level of the MOW water as it spreads westward, agreed well with climatology and limited observations. *Smith et al.* [2000] and *Maltrud and McClean* [2005] have used the 1/10° resolution z-level POP model to simulate the North Atlantic Ocean. In their studies, the MOW penetrates downslope from the sill level (~300–400 m) to only ~500 m depth, while the observed MOW penetrates to ~1100 m. Combined with the poor results of other density current studies using z-level models [*Beckmann and Doscher*, 1997; *Willebrand et al.*, 2001; *Ezer and Mellor*, 2004], z-level models were thought to be poor tools to study density currents. However, *Dietrich et al.* [2004a], *Legg et al.* [2005], and *Drillet et al.* [2005] have shown that with proper numerics, resolution and dissipation, z-level models can give satisfactory results. The recent investigation of the Dynamics of Overflow Mixing and Entrainment (DOME) idealized density current problem using a pure z-level model even shows that the model accuracy, robustness and dissipation play more important role than the chosen coordinate [*Tseng and Dietrich*, 2006].

1.3. Motivation and Approach

[8] Our original goal was to model the currents around the Iberian Peninsula following the supertanker ''Prestige'' oil spill disaster. This required modeling the exchange of North Atlantic and Mediterranean waters through the Strait of Gibraltar, and the associated circulations, including the thermohaline-driven exchange between North Atlantic Ocean and Mediterranean waters (much saltier and denser) through the Strait of Gibraltar, and the descending MOW density current and its deep penetration. Extending the accurate and efficient duo-grid approach in *Dietrich et al.* [2004a], we designed a six-grid, two-way coupled model, MEDiNA (MEDiterranean and North Atlantic) model, in order to satisfy this requirement efficiently. Early on, however, we also recognized the potential climatological importance of the MOW penetration, and encouraged by the model's consistency with previous observations [*Barringer and Price*, 1997], we proceeded to further investigate the MOW dynamics and its effects in the Iberian Peninsula coastal regions.

[9] The challenge of modeling the MOW (see section 1.2) is further amplified when one considers the need for modeling the entire basins: this is required if one wishes to model its large multidecadal timescale effects on climate. MOW is by far the warmest (and most saline) water that accumulates at depth below 1000 m in the North Atlantic, and thus controls its deep ocean heat and salt balance. Extended MOW modeling in the framework of basin-scale, coupled Mediterranean Sea and North Atlantic system has never been done adequately until now. As the results will show (section 3), the choice of this configuration is well justified by the modeled MOW depth and water mass properties agreeing quite closely with the observed climatology.

[10] The MEDiNA model is described in section 2. Section 3 presents the main simulation results, including: (1) MOW/MAW volume exchange rate; (2) MOW downslope migration to its equilibrium depth in the Gulf of Cadiz; (3) MOW flow around the Iberian Peninsula, into the Bay of Biscay; and (4) time mean path around the observed anticyclonic gyre in the far western Mediterranean Sea. Section 4 summarizes concluding remarks and future works.

2. MEDiNA Model: Basic Model and Multiple Grid Framework

[11] To efficiently resolve the Strait of Gibraltar in the fully coupled MEDiNA model, we have employed six grids that are all two-way-coupled to their adjacent grids, each grid being a local Mercator grid. Longitudinal resolution varies from 1/24° in a Strait of Gibraltar regional grid to 1/4° in a central North Atlantic Ocean grid. Brief details of the DieCAST (Dietrich/Center for Air Sea Technology) ocean model, used in this study and based on the primitive equations of incompressible flow, are given in the section below.

2.1. Basic Model

[12] The purely z-level DieCAST ocean model [*Dietrich et al.*, 1987; *Dietrich*, 1997] solves the discretized hydrostatic, incompressible conservation equations that are in integrated ''control volume'' form within each grid. The grids and internal control volumes are coupled by fluxes and pressure forces at their interfaces with adjacent grids and control volumes. All internal control volume fluxes and pressure forces are calculated using interpolations that are rigorously fourth-order-accurate [*Sanderson and Brassington*, 1998; *Dietrich*, 1997], including the linear-exponential stretched vertical coordinate space. No bathymetry smoothing is applied and partial bottom cells are not used.

[13] Subgrid-scale (Reynolds-averaged type) vertical mixing is parameterized by eddy diffusivity (for temperature and salinity) and eddy viscosity (for momentum) using a modified Richardson number approach [*Staneva et al.*, 2001; *Tseng et al.*, 2005] based on *Pacanowski and Philander* [1981]. Common instant convective adjustment is not invoked. Since the horizontal flow is dominated by low dissipation inertial dynamics and water mass advection on all resolved scales, the horizontal cell Reynolds number is extremely large. This, in combination with the high order low dissipation numerics, leads to realistic MOW dilution and associated final equilibrium level. No data assimilation is used, nor any nudging toward climatology which can lead to internal heat and freshwater sources/sinks that do not occur in the real ocean [*Tseng and Breaker*, 2007].

[14] We emphasize that using large or even infinite (such as instant ''convective adjustment'') vertical diffusion in simulating bottom-hugging density currents exacerbates the dispersion errors in z-level models noted above. Density currents migrate downslope over the edges of stairsteps, thus bringing their material over less dense water below. In such cases, the common practice of assuming rapid or instant vertical mixing is physically inappropriate since this makes diffusion dominate the downslope density current propagation leading to excessive entrainment. One must allow downslope propagation to be dominated by modeled horizontal and vertical advection, as occurs in nature. Then a subgrid-scale turbulence closure scheme can represent the mixing and entrainment without being contaminated by numerical errors.

[15] The continuum equations from which the integrated control volume equations are derived are given by *Staneva et al.* [2001]. More model details are available at the model website. The wind-forcing of MEDiNA is obtained from the interpolated monthly Hellerman winds [*Hellerman and Rosenstein*, 1983]. Levitus94 climatology [*Levitus and Boyer*, 1994] is used to initialize MEDiNA and determine its surface sources of heat and fresh water (e-p) using the nondamping precise approach described by *Dietrich et al.* [2004b]. The short-circuited Arctic Ocean is parameterized by an artificial continental shelf along the northern and northeastern boundary; and with a specified freshwater source along the northern boundary. The equatorial boundary condition is slow nudging toward Levitus climatology in a sponge layer. Specified lateral viscosity and diffusivity are 20 m^2/s and background vertical viscosity and diffusivity have maxima of 3.0 and 0.6 cm^2/s in the top layer, decaying exponentially with depth to 0.1 and 0.002 cm^2/s, added to the vertical mixing scheme, to emulate mixed layer effects of storm events not included in the climatological forcing. The bottom is insulated, with nonslip conditions parametrized by a nonlinear drag.

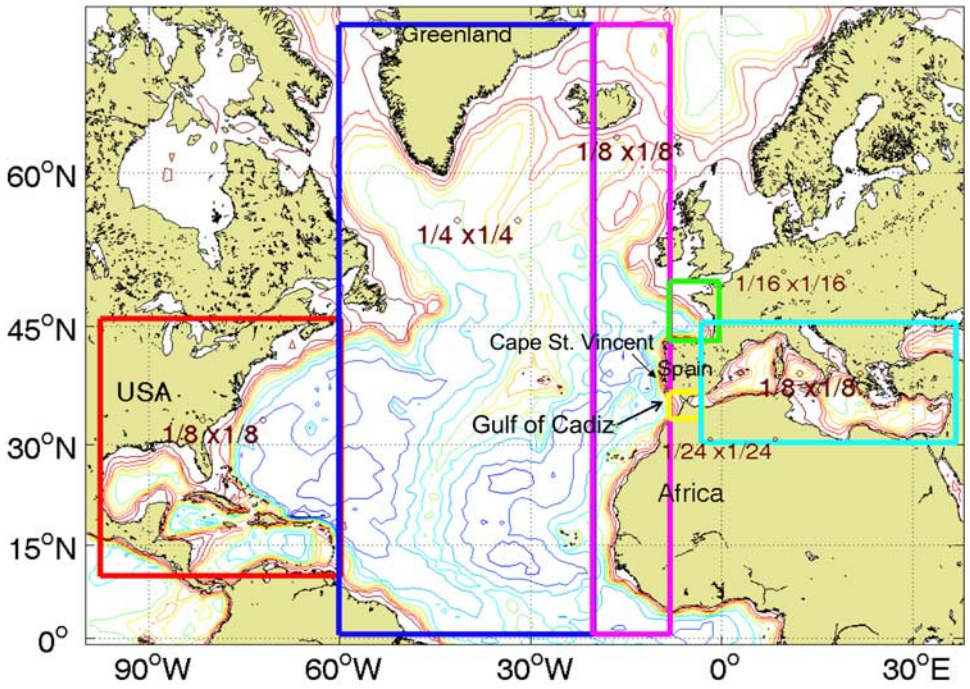

Figure 1. Entire simulation domain of the six-grids MEDiNA model. The grid resolution ranges from 1/4° in the central North Atlantic Ocean grid to 1/24° in the Strait of Gibraltar regional grid. Cape St. Vincent and Gulf of Cadiz are labeled on the map.

[16] Another requirement for accurate simulation of downslope density current migration is the rate of momentum extraction at the bottom layer [*Legg et al.*, 2005; *Tseng and Dietrich*, 2006]. In the absence of such momentum extraction, conservation of absolute potential vorticity strongly inhibits downslope migration and the density current approaches geostrophic balance with the cross-slope pressure gradient. This momentum extraction in its typically thin bottom mixed or ''friction'' layer adds a bottom sink to the along-slope momentum balance, thus generating downslope secondary flows. The nonlinear bottom drag used by the model (using a standard drag coefficient of 0.002) is adequate for that even when the very thin mixed layer at the bottom of the density current is not resolved.

[17] To maintain the observed annual cycle salinity, the rigid lid approximation is slightly modified to allow a model-derived e-p [*Dietrich et al.*, 2004b] be represented by a small vertical velocity at the rigid-lid with no salt flux included (purely freshwater). Thus the rigid-lid is slightly porous, with a nonzero (but extremely small) climatologically based vertical velocity at the slightly porous rigid-lid (see *Dietrich et al.* [2004b] for justification and details). Integrating e-p over the entire Mediterranean Sea gives a net freshwater volume loss at the surface, so the inflow through the Strait of Gibraltar is slightly bigger than the outflow [*Millot*, 2007].

2.2. Multiple Grid Framework

[18] Modeling the Mediterranean Sea near-surface inflow of MAW and underlying outflow of much saltier and denser MOW was made possible by the current multiple grid approach, including a tiny 1/24° resolution Strait of Gibraltar regional grid through which the Mediterranean Sea and North Atlantic are coupled (Figure 1). MEDiNA model has been run for 70 years. Such multiple-grid approach is closely related to the domain-decomposition method described by *Dietrich et al.* [1975] used by the rigid-lid pressure solver [*Roache*, 1995] in a global adaptation of the DieCAST model. The present six-grid model formulation is similar to the duo grid formulation in *Dietrich et al.* [2004a], except we have increased the resolution and replaced the equatorial boundary condition by a conventional sponge layer approach based on climatology. In the future, we will two-way couple the present model to a lower resolution global model.

[19] All six subdomain grids (Figure 1) share the same smoothly stretched (linear-exponential) z-level vertical grid. Within each individual grid (all in a spherical coordinate framework), longitudinal resolution is uniform and latitudinal resolution is generated such that varying latitude and longitude grid increments are equal everywhere (Mercator grid). Lateral resolutions and grid sizes for all six grids are summarized in Table 1. The vertical resolution is a linear-exponential stretched grid of 30 layers, with a 10 m thick top layer. The vertical grid is graphically indicated in the vertical cross-section plots presented.

Table 1. Lateral Resolution and Grid Size in Each Grid

Domain	Lateral Grid Resolution	Grid Sizes
Western North Atlantic	1/8°	302 × 334
Central North Atlantic	1/4°	160 × 396
Eastern North Atlantic	1/8°	98 × 792
Bay of Biscay	1/16°	112 × 156
Strait of Gibraltar	1/24°	123 × 105
Mediterranean Sea	1/8°	314 × 155

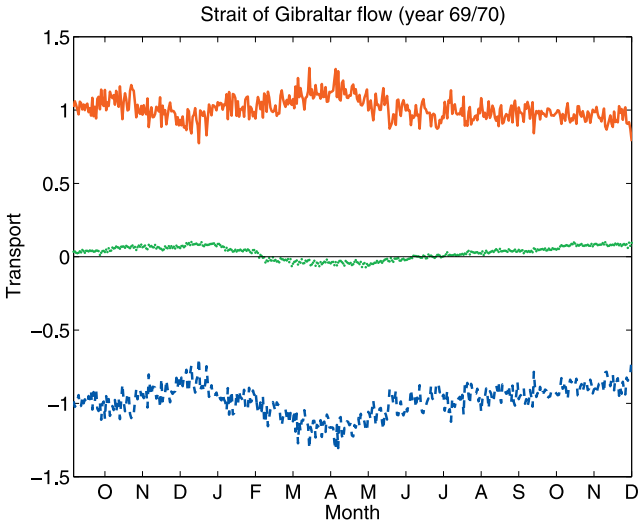

Figure 2. Transport through the Strait of Gibraltar during the last part of year 69 and all of year 70, computed from daily model data in the choke point cross-section having about 50 points. The red (blue) curve shows the total eastward (westward) volume flow integrated over all points having eastward (westward) flow; the green curve is the sum of the blue and red curves.

[20] The grid coupling approach includes upwind-based cross-intergrid-boundary fluxes, as did the approach used by *Dietrich et al.* [2004a]. The commonly used time filter (timescale of a few days) has little effect on the coupling other than to damp high frequency internal modes of the finer of two adjacent grids that are not resolved by the adjacent two-way-coupled coarser grid. The resulting grid coupling is nearly seamless with low diffusion and viscosity. No intergrid sponge layers are applied.

3. Simulation Results

[21] The Levitus'94 climatology [*Levitus and Boyer*, 1994] that is used to initialize the MEDiNA model does not resolve the Strait of Gibraltar. Even if it did, the flow through the strait is not balanced [*Viudez et al.*, 1998] and thus cannot be accurately initialized from water mass climatology. Thus for simplicity, the model was initialized with no flow everywhere on all six grids.

[22] Using varying resolutions in a bigger region and simulating multiple decades, the present MEDiNA model produces results very similar to those reported by *Drillet et al.* [2005]. Further comparisons are made of the depths and westward penetration longitudes of the core salinity with analyses based on climatology by *Iorga and Lozier* [1999]. In regions closer to Gibraltar and the Spanish coast, for longitudes <10°W, comparisons are also made with observations and model results by *Bascheck et al.* [2001] and by *Johnson et al.* [2002]. These results are discussed in sections 3.1–3.3 below.

3.1. Water Mass Exchange Through Strait of Gibraltar and Associated Currents

[23] After a few model years, a westward 1 ± 0.05 Sv MOW flow through the Strait of Gibraltar occurs throughout the model simulation. Above it, an eastward 1.1 ± 0.1 Sv MAW flow occurs. These match well with the values inferred from the observations within observational error [*Bascheck et al.*, 2001]. This energy-intensive water mass exchange through the narrow Strait of Gibraltar strongly affects the Iberian Peninsula coastal regions, and also significantly affects the entire Mediterranean Sea. Agreeing with observations, the simulated eastward volume flow is generally larger than the westward flow because it must balance the freshwater sink (based on the surface freshwater flux treatment described by *Dietrich et al.* [2004b]) due to the net effects of rivers, precipitation and evaporation.

[24] Figure 2 shows the daily transport through the Strait of Gibraltar during the last part of year 69 and all of year 70 in the choke point cross-section (∼50 model grid points). The red (blue) curve shows the total eastward (westward) volume flow integrated over all points having eastward (westward) flow; the green curve is the sum of the total transport. The sum represents the total inflow through the Strait of Gibraltar into the Mediterranean Sea, whose long term average exactly balances the e-p-river sources to maintain Mediterranean Sea surface level; rigid-lid approximation enforces this balance each time step. Thus the green curve may be compared with an average annual cycle e-p-river sources based on climatological data mostly before the Aswan dam and other uses of Mediterranean Sea rivers for irrigation decreased the river inflows. There is a 3–5 d fluctuation of the inflow and outflow which are almost exactly opposite, with the small residual containing the smoothly varying annual cycle e-p-river sources shown by the green curve.

[25] The time average westward transport (blue curve) is about 1 Sv and is the MOW source. The time average eastward transport (red curve) is slightly bigger (by about 0.03 Sv), most clearly shown by the green curve, due to the time average e-p-river sources in the Mediterranean Sea (time average of the green curve) and is the fresher MAW source to the Mediterranean Sea. The e-p-river sources maximum is about 0.1 Sv during January, but switches sign to about −0.02 Sv during the spring. In nature, these may be affected by slight fluctuations of the total Mediterranean Seawater volume (lateral mean surface height) that cannot be modeled using a rigid-lid approximation, but may have very little effect on the Mediterranean Sea general circulation. In our earlier stand-alone Mediterranean Sea studies using the present model, we found (not reported) that even the implied regional vortex stretching associated with the locally big e-p in the eastern Mediterranean Sea has little effect on its regional circulation, indicating that the rigid-lid approximation is appropriate [*Fernandez et al.*, 2005]. There is significant interannual variability even though the model is forced by exactly repeating annual cycle climatological data and is well converged after long years of integration.

[26] Figure 3 shows the annual averaged velocity at 1000 m depth superposed on the time averaged surface height in the Strait of Gibraltar regional grid during year 20. It clearly shows that deep flows west of the Strait of Gibraltar cross the surface height contours. The flow is nearly geostrophic at all levels outside the top and bottom boundary layers and a slightly supergeostrophic flow in the Strait [*Viudez et al.*, 1998]. Thus this indicates the baroclinic nature of the flow.

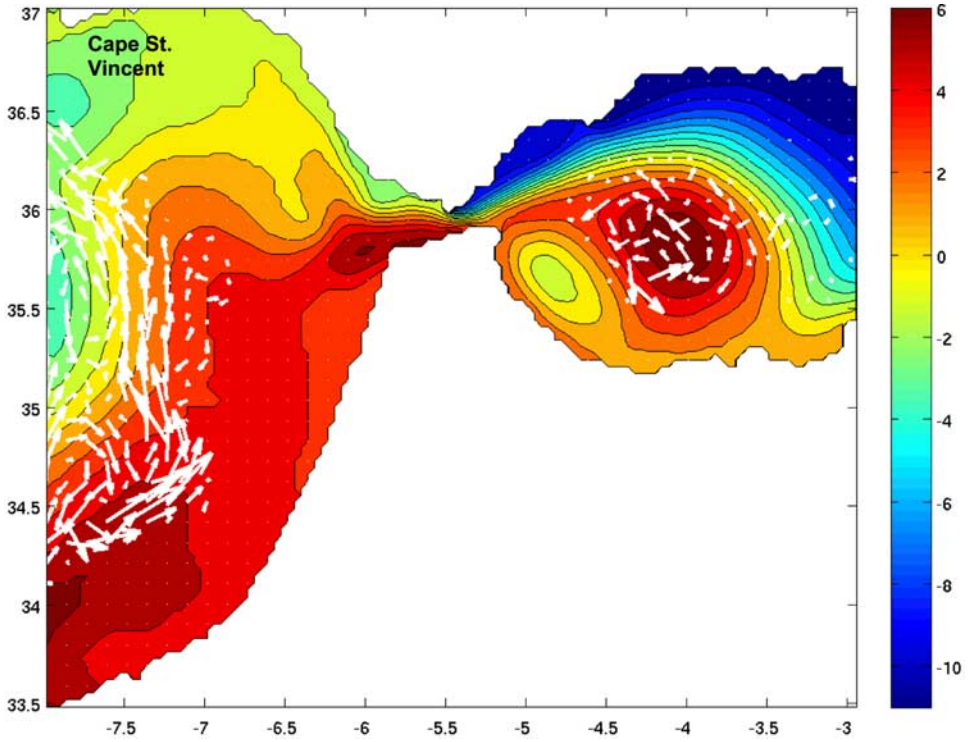

Figure 3. Annual averaged sea surface height (color contours) and 1000 m depth velocity vectors in 1/24° resolution Strait of Gibraltar regional grid during year 20. The maximum velocity magnitude is 48.9 cm/s. The unit of sea surface height is cm. Longitude (°) is shown in x axis while latitude (°) is shown in y axis.

The NAW freshwater jet east of the Strait is similar to the observed jets [*Viudez et al.*, 1998] and other high resolution model results [e.g., *Drillet et al.*, 2005]. In spite of using a rigid-lid approximation which excludes the fluctuations due to tides, the time average water mass exchange is consistent with observations [*Bascheck et al.*, 2001], thus providing a realistic Strait of Gibraltar upstream condition for the MOW density current. The interface between the MOW and the MAW is near the observed depth ranging from 50 to 200 m [*Tintore et al.*, 1988]. The MAW forms a surface layer characterized by salinities that increase, due to evaporation and mixing, from 36.5 at the Strait of Gibraltar to 38.0–38.3 in the north of the Western Mediterranean Sea, and by a mean temperature, below the mixed layer, of 14–15° [*Millot*, 1999]. The interface between the MAW and MOW in the Strait of Gibraltar is ~60–100 m thick with a strong vertical salinity gradient. The interface is thicker, deeper and fresher (colder) on the west end of the Strait [*Bray et al.*, 1995]. The MOW water mass properties are also very close to the climatology as shown later.

[27] Note that this water mass exchange through the Strait of Gibraltar is obtained with no data assimilation in spite of the coarse Strait of Gibraltar resolution. The water mass exchange relies on the throughflow dynamics and is critical for long term climate change since the MOW has significant impacts on the deep and intermediate heat and salt balance in the North Atlantic Ocean.

3.2. MOW Spawned Density Current West of Gibraltar

[28] Figure 4 shows instantaneous vertical/latitudinal cross-sections of model results in the 1/24° resolution Strait of Gibraltar regional grid at the end of year 20. Figures 4a–4e show Strait of Gibraltar regional grid results (at 8.1°W), just east of its interface with the 1/8° resolution eastern North Atlantic grid. The deep MOW is clearly visible along the Iberian slope around 1000 m depth in the (Figure 4a) longitudinal velocity, (Figure 4b) latitudinal velocity, (Figure 4c) salinity, (Figure 4d) temperature and (Figure 4e) vertical velocity. The present results compare well with those of *Johnson et al.* [2002] at 8.25°W (their Figure 3). Note that the unfiltered 1/24° resolution bathymetry is used herein. The MOW reaches the equilibrium depth at ~1000 m just upstream of this longitude, as shown by vertical sections east of this longitude (Figures 4f–4i; Figure 4i is in the westernmost of the Strait).

[29] The material elements flow along the bottom slope for O(10) days between the Strait and Cape St. Vincent just west of 8.1°W (Figures 4a–4e). They approach their equilibrium depth just east of 8.1° W, after entraining some North Atlantic water between the Strait and 8.1° W. Some of the MOW material spreads offshore, away from the bottom slope, thus getting sandwiched by the much less saline and colder ambient North Atlantic water. This may involve weak frictionally induced secondary flows in the

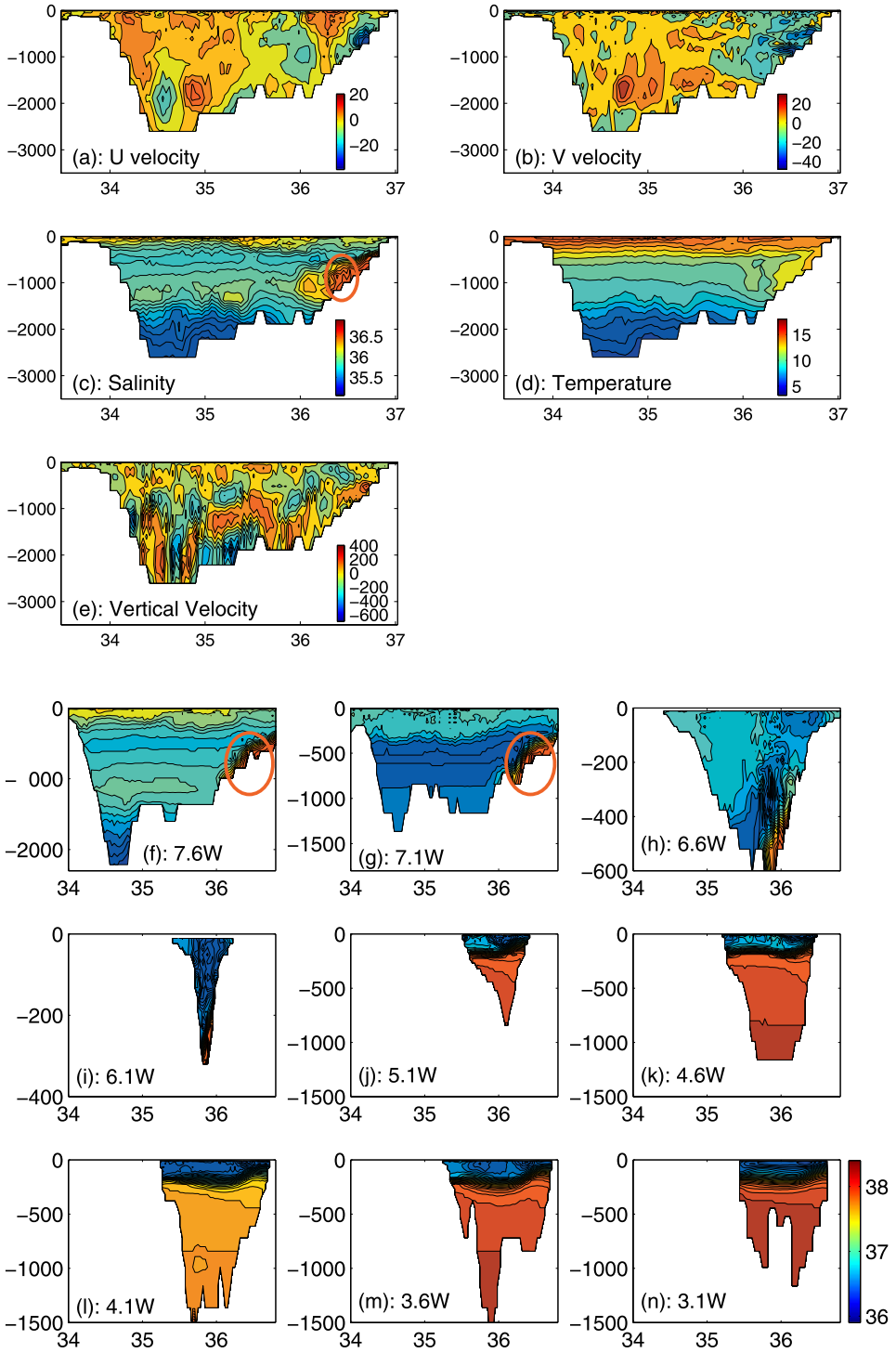

Figure 4. Vertical/latitudinal sections from the 1/24° resolution Strait of Gibraltar regional grid at the end of year 20. Figures 4a–4e are at 8.1°W longitude, which is the model longitude adjacent to a 3-zone overlap region between the 1/8° resolution eastern North Atlantic grid and the Strait of Gibraltar regional grid (Figure 1). Figures 4a–4e show longitudinal velocity (positive eastward), latitudinal velocity (positive northward), salinity, temperature and vertical velocity (positive downward, in m/d), respectively. Figures 4f–4n show salinity every 1/2° going eastward from Figure 4c, except the extremely narrow Strait of Gibraltar choke point. 10° water is seen as deep as 1300 m. Figures 4j–4n show the thin near-surface relatively fresh layer of North Atlantic water east of the Strait. This sequence shows the downslope MOW flow as a result of secondary flows in the bottom friction layer as one goes westward from the Strait of Gibraltar, reaching its equilibrium depth (∼1000 m) in the westernmost longitude (Figures 4a–4e) where it begins its offshore spread. Dense MOW is marked as circles. Longitude (°) is shown in *x* axis while depth (m) is shown in *y* axis.

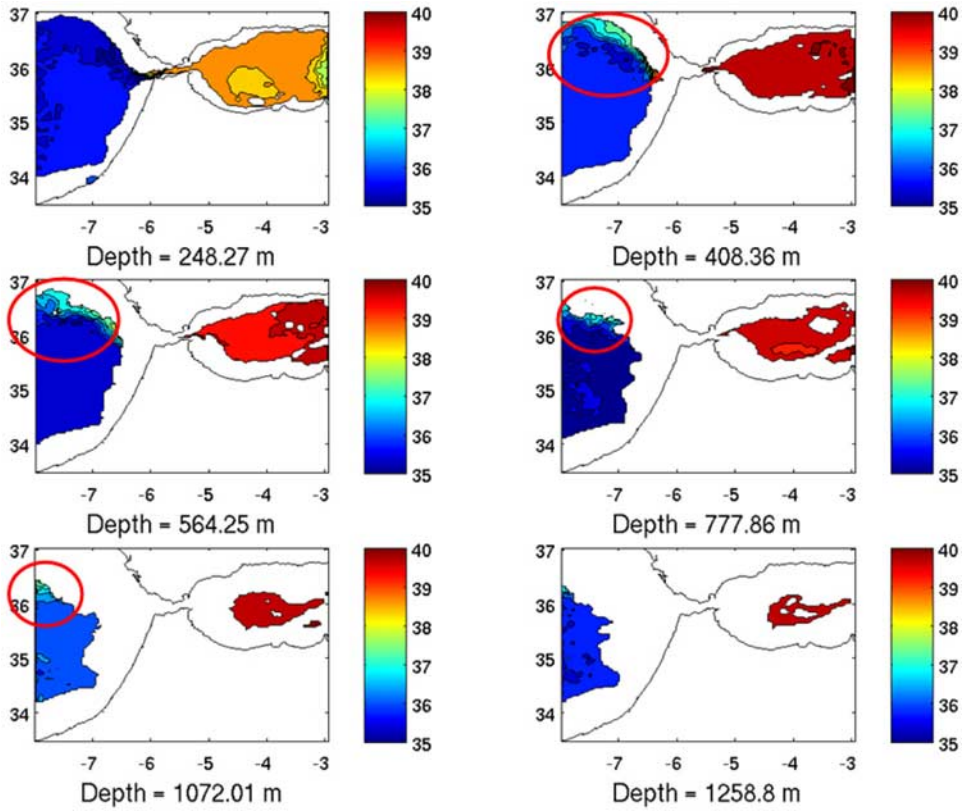

Figure 5. Salinity at the end of year 20 in the 1/24° resolution Strait of Gibraltar regional grid at various depths. Dense MOW is marked as circles. The unit of color contours is g/kg. Longitude (°) is shown in x axis while latitude (°) is shown in y axis.

open water (away from the bottom) as well as upstream fluid dynamic instabilities.

[30] Figures 4j–4n focus on the totally different behavior east of the Strait (Figure 4j locates at longitude 5.1°W). It is dominated by a thin near surface eastward flowing plume of MAW overriding much saltier westward flowing Mediterranean Seawater; the upper part of the latter spills over the Strait' sill around 300–400 m depth, some of it having upwelled as bottom-drag-induced secondary flows in the dominant anticyclonic gyre east of the Strait, probably with the help of the cyclonic frontal eddies. The energy intensive Strait of Gibraltar region is externally forced by the big scale buoyancy differences between the North Atlantic and Mediterranean Seawater masses and is a focal point of multiscale nonlinear interactions.

[31] Figures 4f–4i, spaced uniformly between 8.1°W and the Strait of Gibraltar, continuously show the high salinity intense MOW bottom density current jet core location downstream from the Strait of Gibraltar sill. The modeled MOW forms an intense downstream jet from a thin, narrow Strait of Gibraltar sill source. After approaching a near balance among Coriolis, buoyancy and viscous forces, the horizontal flow is nearly parallel to depth contours except near the bottom [*Tseng and Dietrich*, 2006]. The MOW density current gradually edges downslope as it flows westward from its Strait of Gibraltar source (the sill saddle point over which it flows near the bottom is around 300–400 m depth). A high salinity region occurs at deeper levels away from the Strait of Gibraltar and is marked as circles. This descent of the MOW density current reflects secondary downslope flows in the bottom friction layer as it flows westward until reaching the equilibrium depth, where it matches the ambient NACW density and begins mixing and spreading over deeper, less saline NACW away from the bottom slope. Along the way, its salinity decreases due to NACW entrainment and vertical mixing parameterization. Note that the 10°C water can be observed as deep as 1300 m.

[32] Near Cape St. Vincent (shown in Figure 3), the main MOW core turns northward and flows along the North Atlantic coast of Spain as it slowly spreads offshore, entrains NACW and mixes vertically. However, the MOW density current remains concentrated near the Iberian Peninsula coast and near its equilibrium level as it flows northward in the 1/8° resolution eastern North Atlantic Ocean grid, finally turning into the Bay of Biscay.

[33] To further reveal the structure of the MOW density current near its Strait of Gibraltar source, Figure 5 shows horizontal plots of salinity at various levels of the Strait of Gibraltar regional grid at the end of year 20, thus complementing the results in Figure 3 for the MOW density current downslope penetration. Salty MOW is highlighted with circles at different depths. These details show the descent and spreading behavior of MOW to be consistent with observations [e.g., Figures 1 and 5a of *Barringer and Price*, 1997].

[34] Figure 6 shows the annually averaged vertical/latitudinal plot of salinity in Bay of Biscay at longitude of

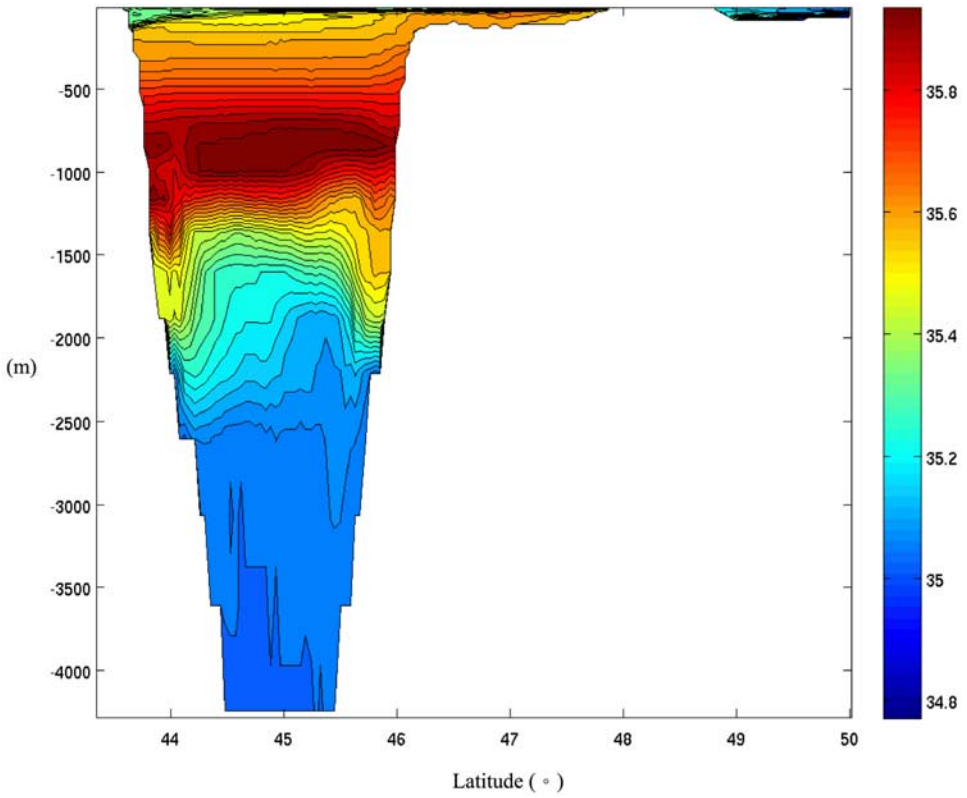

Figure 6. Annual averaged vertical/latitudinal plot of salinity in Bay of Biscay at longitude of Santander (3.8°W) shows salty MOW in intermediate depths during year 20. The Prestige oil spill in deep water off the NW corner of the Iberian Peninsula polluted its entire north coast, as consistent with this figure. Combined with Figure 4, this indicates MOW flow path from the oil spill region to the Bay of Biscay; the same currents may entrain and transport the leaking, slowly rising oil into the Bay of Biscay. Latitude (°) is shown in x axis while depth (m) is shown in y axis.

Santander (3.8°W) during year 20. It took around 5 years for the MOW to penetrate northward and turn eastward into to the Bay of Biscay. After turning northward at the southwest corner of the Iberian Peninsula near Cape St. Vincent, the MOW spread laterally and shed some anticyclonic deep eddies, thus slowing its northward penetration. It also slowly entrained North Atlantic water, thus diluting it, but the MOW signal is evident all along the Iberian west coast and well into the Bay of Biscay (Figures 4–6).

[35] Figure 7 shows the annual averaged bottom boundary layer in the Gibraltar regional grid during year 20. The sloping bottom boundary layer is the boundary cell just above the topography where the depth is less than 1075 m and at uniformly 1075 m deep where the depth is greater than 1075 m. Figures 7a–7d show horizontal velocity vectors superposed on depth contours, bottom salinity and temperature, and vertical velocity. These plots illustrate MOW density current downslope migration, dilution and spreading at 1075 m depth (near its observed equilibrium level). The strongest downslope flow (positive vertical velocity contours, shown in solid, indicate descending flow) is along very steep bathymetry immediately downstream of the Strait of Gibraltar (Figure 7d).

[36] Note that a large Gulf of Cadiz abutment jutting southwestward from the shelf break at the ~500 m depth exists just upstream of Cape St. Vincent. Figure 7 also indicates the strong MOW interaction with that abutment. The abutment's base is 500–900 m depth, which is large enough (~10 × 30 km scale, Figure 7a) to invoke a significant rotational constraint on the MOW flowing over it from deeper levels toward its equilibrium depth. The offshore edge of the abutment is steep, dropping rapidly to ~900 m depth. Its southwest-northeast oriented ridgeline is normal to far field large-scale shelf-slope contours. As the MOW density current approaches from the east, much of it is deflected southwestward rather than flowing over the abutment (see Figure 7a) due to rotational and buoyancy constraints. Some other MOW flows over the abutment and along the shallower shelf-slope. Thus the MOW is split into a shallow nearshore branch and a deeper offshore branch by the interaction with this abutment. The southwestward deflection of MOW results in an intense current along the steep southwestern edge of the abutment, where bottom drag generates large lateral shear with negative relative vorticity such that the absolute vorticity is negative. Thus the rotational constraint on the propagating water is eliminated locally near its southwestern edge. A turbulent wake results from the rapid release of any residual available potential energy that remains from its Strait of Gibraltar source [*Tseng and Ferziger*, 2001]. The abutment-induced shear thus augments the anticyclonic vorticity generated by the MOW spreading near its equilibrium level. This results

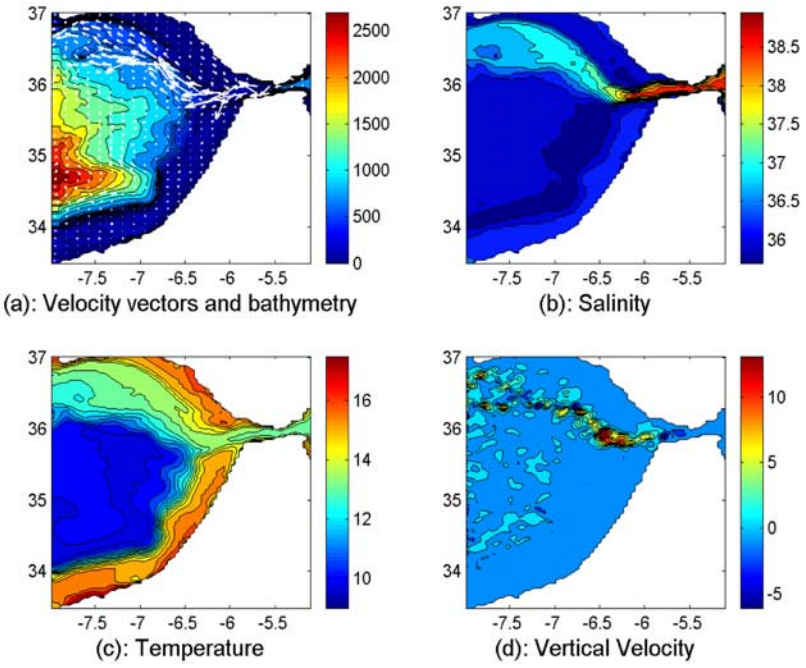

Figure 7. Annual averaged deep flow west of the Strait of Gibraltar in the 1/24° resolution Gibraltar regional grid at year 20. For depth shallower (deeper) than 1075 m, time averaged bottom field (depth 1075 m horizontal field) is shown. (a) Horizontal velocity vectors and depth contours (the unit is meter); (b) Salinity; (c) Temperature; (d) Vertical velocity. Longitude (°) is shown in *x* axis while latitude (°) is shown in *y* axis.

in a ''bull's-eye'' in the eddy kinetic energy contours downstream from the steep southwestern tip of the abutment (Figure 8a).

[37] The anticyclonically rotating MOW elements in the turbulent wake of the abutment spread as they geostrophically adjust and merge. The adjustment occurs in scales comparable to the local *Ro*. MOW accumulates slightly above and below the equilibrium level before anticyclonic meddies break away, thus maintaining a finite MOW thickness [*Drillet et al.*, 2005]. Viewing the meddies as ''floating water mass elements'' in an ambient density stratified flow, the water above (below) the equilibrium level is denser (lighter) than the laterally ambient water. It follows that the thermal wind above and below the equilibrium level is such that the deep MOW signal decreases away from that level. Indeed, Figure 8b shows that the signal from this abutment is relatively weak near the surface.

[38] Thus the MOW interaction with the steep abutment bathymetry, combined with buoyancy induced MOW spreading, augments the MOW anticyclonic vorticity. Having descended toward its equilibrium level by the time it reaches the western Gulf of Cadiz, the MOW spreads toward deeper water and clockwise around the Iberian Peninsula coast, as seen in Figures 4, 5, and 7.

[39] Along the Iberian Peninsula west coast, south of 43°N, the modeled MOW is not only close to GDEM climatology but also quite similar to the upper level flow shown in Figure 5b of *Johnson et al.* [2002], although they used higher resolution (1/24° and 36 vertical layers, with depth truncated at 2000 m) in a focused southwestern Iberian Peninsula coastal region model.

3.3. Penetration of MOW Waters Into the North Atlantic

[40] The modeled MOW water mass, concentrated near 1000 m depth, is clearly observed in the vertical/longitudinal salinity cross-section at 43°N (Figure 9) and in the vertical/latitudinal cross-section at 15°W (Figure 10). In this section, we will make comparisons with climatology (GDEM and *Iorga and Lozier* [1999]) and other model results [*Drillet et al.*, 2005].

[41] Figure 9 compares the annual averaged model salinity (a) with the U. S. Navy's Generalized Digital Environmental Model (GDEM) 1/4° resolution climatology (b). The early version of the GDEM climatology has been compared with Levitus climatology [*Teague et al.*, 1990]. This later version of GDEM appears to render better representations of seasonal variability and high shear regions due to a different smoothing method and a finer grid spacing. The consistency implies realistic MOW density current penetration, dilution and propagation, for both climatology and the 1/8° resolu- resolution model. The 35.8 isohaline penetrates to ∼16°W in GDEM and to ∼18°W in the model. The thickness of the high salinity core with depth, as defined by this isohaline, is ∼800 m for GDEM and ∼780 m for the model at 10°W. The mean depth for the GDEM core is ∼900 m, and for the model is ∼1000 m. *Iorga and Lozier* [1999] [hereafter IL99] present a similar salinity field (their Figure 15a) along 46°N; the mean depth of the *Lozier et al.* [1995] climatology at this latitude is ∼1000 m. Its thickness with depth is difficult to estimate, since the 35.7 isohaline seems to form eddy-like structures at 12°W and 8°W. Thicknesses at those longitudes are ∼400 m at both locations. We note in passing

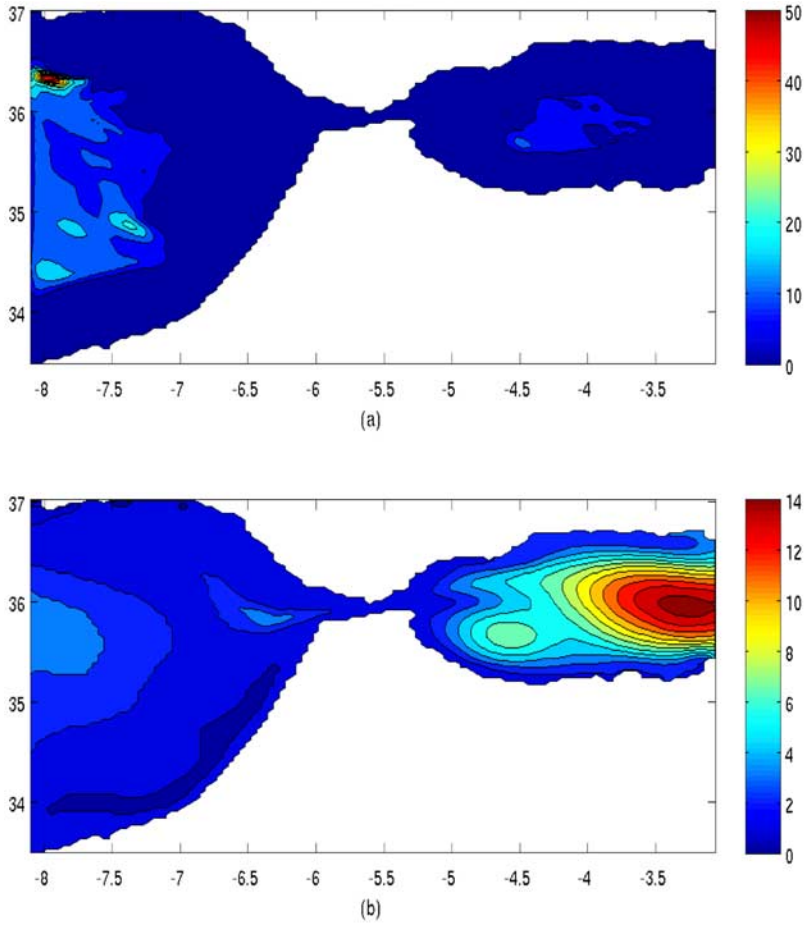

Figure 8. Annual averaged eddy kinetic energy and sea surface height anomaly in the 1/24° resolution Gibraltar regional grid during year 20. (a) RMS velocity anomaly (root mean squared deviation of horizontal velocity from its time average) at 1000 m depth; bull's-eye reflects turbulent wake of MOW flow diverted around mesa-like seamount seen in Figure 6a. The unit of color contours is cm/s. (b) RMS of sea surface height deviation from its time average; dominated by the eastward low density MAW overriding the westward MOW through the Strait of Gibraltar, and the resulting energetic western Alboran Sea anticyclonic gyres and associated cyclonic eddies. The unit of color contours is cm. Longitude (°) is shown in *x* axis while latitude (°) is shown in *y* axis.

that GDEM seems to have a weak eddy formed at 11°W with the 36.0 isohaline.

[42] Finally, we compare these with the model results of *Drillet et al.* [2005] [hereafter DR05], who used daily ECMWF wind-forcing from 1998–2002, with a mean resolution of about 5 km and 43 levels. In addition, they had to use some assimilation of climatology in the Gulf of Cadiz region to improve the correct sinking rate. Their mean depth for the core defined by the 35.8 isohaline is ~850 m, and its thickness at 10°W is ~700 m (versus 1000 m and 780 m for the present modeled depth and thickness, respectively).

[43] As noted by both IL99 and DR05, there appear to be multiple advective pathways of MOW water present in the Mid-Atlantic that change with longitude. Figure 10 shows the vertical cross-sections for the longitudinal velocity U and salinity S, along 15°W. At this longitude, the flow is relatively free from the immediate topographic-coastal influences of the Iberian Peninsula Coast, and gives an insight into the main penetration of the MOW into the North Atlantic. Similar results are displayed from climatology by IL99 at 15°W for S (their Figure 11b), and from simulations by DR05 for S (their Figure 4b) and U (their Figures 7 and 8).

[44] The main difference between these figures is the appearance in the present results (Figure 10) of three distinct jets (defined by the 36.2 isohaline), centered on the 950 m depth level, and on longitudes 36.7°W, 39.2°W, and 43.4°W, respectively. In Figure 11b of IL99, there appear two jets, centered on the 1000 m depth level. The first one, centered on 36.6°W, appears well-defined and strong, the second, centered on 39.2°W, appears quite weak. These seem to correspond to the southern two jets of the present simulations, but with the second one very weak in climatology. In Figure 4b of DR05 there appears to be one jet defined by the 36.2 isohaline, centered on the 850 m depth level and on the 38.9°W longitude. This seems to correspond to our jet centered on the 39.2°W latitude. The fact that these jets appear also in climatology, in the 3-year average of the DR05 simulations and the annual average of the present calculations, suggests that these are not transient

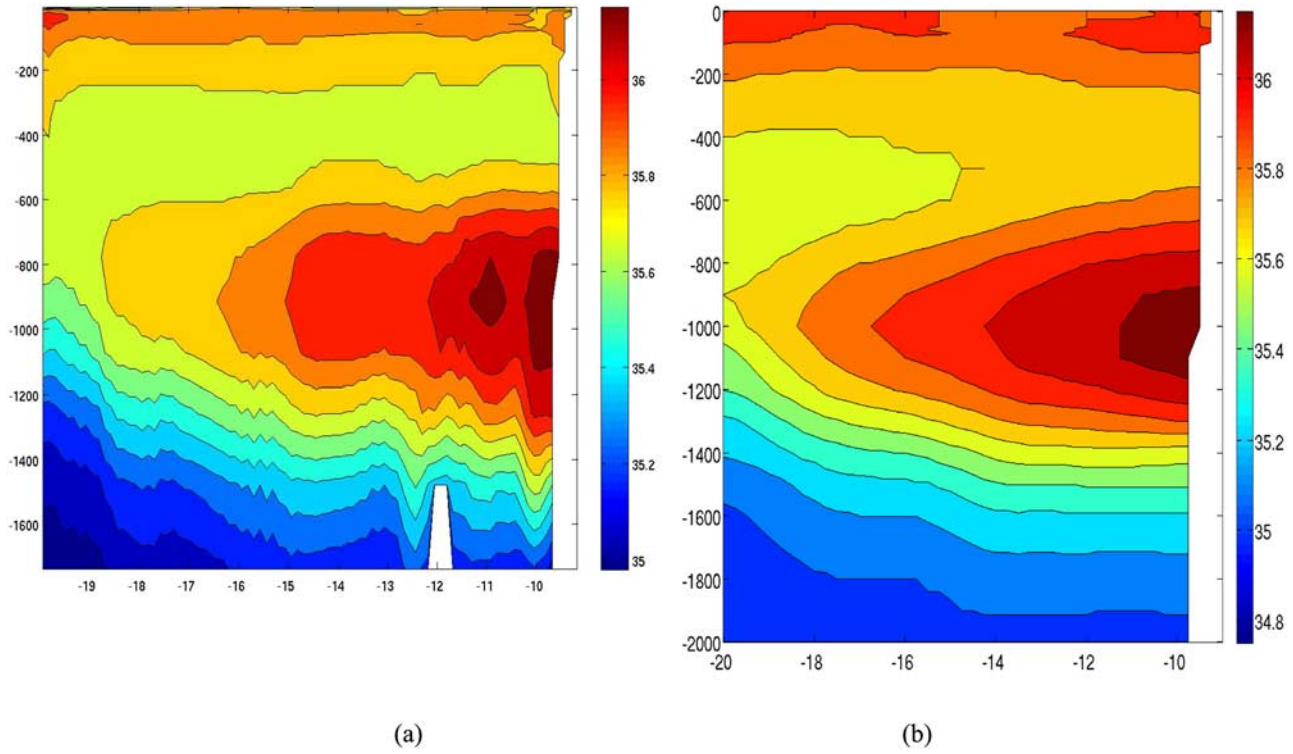

Figure 9. Vertical/longitudinal salinity section at 43°N. (a) the annual averaged model results, showing only upper 24 model levels (scaled to compare with Figure 9b) and (b) U. S. Navy's GDEM climatology. The unit of color contours is g/kg. Longitude (°) is shown in *x* axis while depth (m) is shown in *y* axis.

meddies but manifestations of a more permanent westward advective phenomenon, though probably fluctuating in location (depth, latitude), and in magnitude with longitude. This will be further discussed in the next paragraphs below in connection with the advective veins of velocity.

[45] An examination of the figures for U shows the presence of distinct "veins" of westerly motion in both models. The veins in Figure 7 of DR05, labeled 1 and 2, and an unlabeled vein between veins 3 and D, are centered on longitudes 36.3, 38.7, and 43.3°W, respectively, and appear to have close alignments with the salinity jets of our Figure 10b centered on latitudes 36.7, 39.2, and 43.4°W. Figure 10a of the present paper shows the presence of a weak vein at latitudes 36.2, a stronger one at 38.7, and very strong one at 43.0°W. A further examination of these two figures shows the flows in DR05 to be much stronger, but the latitudinal locations are very close.

[46] We note that although Figure 7 of DR05 is centered on 15°W, it actually shows a diagonal cross-section from 20°W to 10°W. This may explain the fact that the correlation between their velocity veins and our salinity jets is better than with the velocity veins in our Figure 10a, since the advective effects in the north-south direction and fluctuations along longitudes can have significant influences. These effects in fact can be seen clearly in Figure 8 of DR05 for the horizontal velocities at 870 m depth. In the domain covering 30–50°W and 30–50°N, one clearly notes oscillations in the current paths, with the currents maintaining a large degree of connectivity. These path oscillations can explain some of the latitudinal position changes of the veins discussed above, and some of the longitudinal amplitude changes.

4. Summary and Concluding Remarks

[47] This study is especially notable because the MEDINA model integration was accomplished using a single processor Pentium 4 based personal computer (PC). It is a full Mediterranean Sea/North Atlantic/Caribbean Sea/Gulf of Mexico system coupled ocean model. Furthermore, it used a purely z-level model to resolve multiscale dynamics without data assimilation or nudging to climatology. The detailed physical dynamics are resolved by the numerical integration. The main simulation results are.

[48] (1) MOW/MAW volume exchange rate near the observed ~1.0 Sv transport.

[49] (2) MOW downslope migration to its observed ~1 km equilibrium depth in the Gulf of Cadiz.

[50] (3) MOW flow around the Iberian Peninsula (into the Bay of Biscay) and its ability to spread into the 1/8° reso- resolution eastern North Atlantic grid, and even into a 1/16° resolution Bay of Biscay grid.

[51] (4) MOW salt core (S > 35.7) penetration to 18°W.

[52] (5) The meandering MAW jet and the time mean path around the anticyclonic gyre in the western Mediterranean Sea.

[53] This study also showed the MOW interaction with a large abutment, and its spreading near the equilibrium level westward and northward toward observed longitudes and latitudes. In general, the simulated results and dynamics agreed well with observations. These results were noteworthy

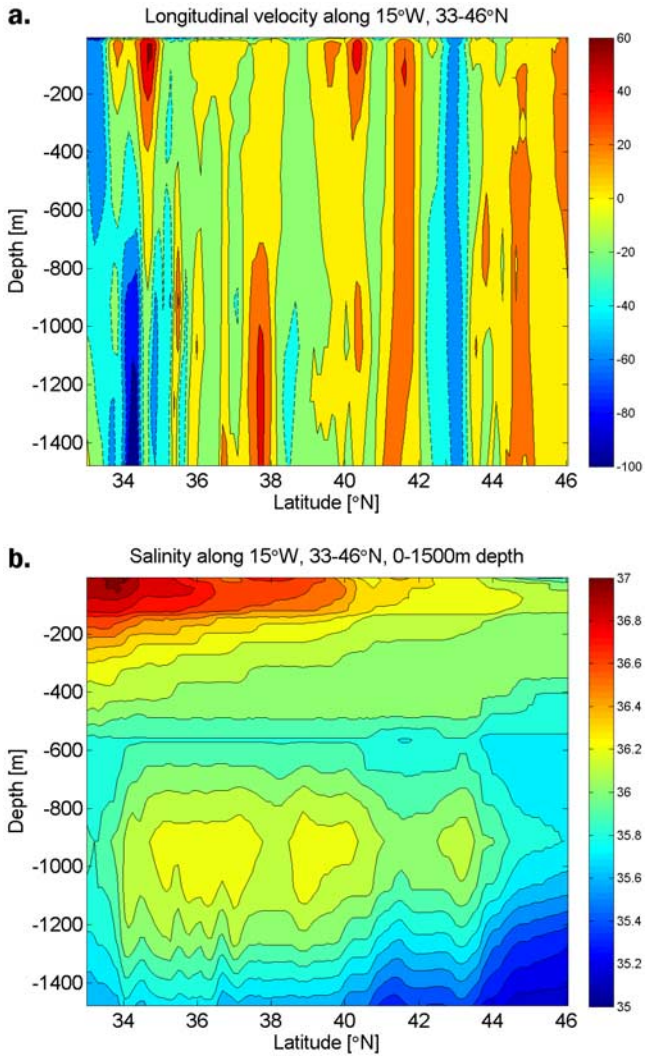

Figure 10. Vertical/latitudinal cross-sections of longitudinal velocity component U (a) and salinity S (b) at 15°W from the annual averaged model results. Only upper 24 model levels are shown (down to 1450 m). Latitude ranges 33–46°N. Unit of salinity is g/kg, and the unit of velocity is mm/s.

since the Strait of Gibraltar sill choke point is resolved laterally by four model control volumes (grid points) in the surface layer and fewer in the bottom few layers through which dense MOW clearly "spills over the dam". We have also demonstrated that the present multiple grid approach, combined with the lack of excessive dilution of density currents, allows modeling fine-scale features such as the Strait of Gibraltar and its associated MOW density current in the multibasin-scale model framework. Such multiple grid approach may be applied judiciously to take advantage of parallel computing power, although the present results were all obtained on a single processor PC in a reasonable time frame.

[54] We also emphasize on the importance and the requirement of maintaining the intense MOW density currents without excessive dilution. Invoking some diffusive treatments such as instant "convective" adjustment in the bottom two layers of z-level models is simply inappropriate physics for modeling bottom-hugging density currents (which flow with little dilution over an insulated bottom); see the discussion by *Tseng and Dietrich* [2006]. Such approach does not allow advection to realistically dominate downslope density current migration–diffusion, dilution and entrainment being secondary albeit critical processes to model realistically.

[55] In the past, some z-level models did poorly in modeling density currents and this has been taken to imply that this is an inherent feature of all z-level models. This conclusion is found to be premature, based on an incomplete survey of z-level ocean model studies under way [e.g., *Johnson et al.*, 2002; *Dietrich et al.*, 2004a; *Legg et al.*, 2005; *Drillet et al.*, 2005; *Tseng and Dietrich*, 2006]. Some of the past problems of z-level models could be attributed to an excessively diffusive behavior resulting from the model's numerics (nonrobust numerical approximations that require large dissipation to avoid excessive computational noise and/or numerical instability), or a combination of incomplete physics and numerics. The current study suggests that it was these factors, rather than the coordinate system, that caused the poor performance.

[56] On the basis of the accurate MOW transport simulation in this paper, it seems possible to address long term effects (decade to century timescale) of MOW on North Atlantic Ocean water masses and Arctic Ocean ice dynamics using a coupled Mediterranean Sea/North Atlantic Ocean/Arctic Ocean model; this requires a straightforward extension of the present model with added ice dynamics. These long term effects include the evolution of the Mediterranean Seawater mass properties through directly specifying the river sources rather than deriving them from the model and climatology as done here. They also include assessing likely positive biogeochemical feedbacks [*Lai et al.*, 2005]. Such feedbacks may be significant because: there is more than enough chemical energy in known slightly buoyant methane hydrates loosely held in the ocean sediments to melt all of the world ocean ice; and biogeochemical processes in deep ocean ecosystems can metabolically oxidize ("ocean slow burn") methane gas in bubbles that form when the hydrate dissociates due to exposure to warmer currents and the methane gas product escapes from bottom sediments into the overlying water [*Lai et al.*, 2005]. This and other ocean biogeochemical dynamic effects on the ocean water masses can be inferred from observed chemical species distributions in the ocean [*Lai*, 2006] and are challenging subjects for future research.

[57] **Acknowledgments.** This project was supported by the Marcelino Botin Foundation and by AcuSea, Inc. The authors acknowledge the support from National Science Council, Taiwan (grant NSC 962618M002010 and 962811M002069) and computing resource of National Center for High-Performance Computing, Taiwan. Useful suggestions and comments on improving the text by Robert Haney, the editor, and three anonymous reviewers are gratefully acknowledged.

References

Barringer, M., and J. F. Price (1997), Mixing and spreading of the Mediterranean Overflow, *J. Phys. Oceanogr.*, *27*, 1654–1677.

Bascheck, B., U. Send, J. G. Lafuente, and J. Candela (2001), Transport estimates in the Strait of Gibraltar with a tidal inverse model, *J. Geophys. Res.*, *106*, 31,017–31,032.

Beckmann, A., and R. Doscher (1997), A method for improved representation of dense water spreading over topography in geopotential-coordinate models, *Phys. Oceanogr.*, *27*, 581–591.

Bethoux, J.-P., B. Gentili, and D. Tailliez (1998), Warming and freshwater budget change in the Mediterranean since the 1940s, their possible relation to the greenhouse effect, *Geophys. Res. Lett.*, *25*, 1023–1026.

Bray, N. A., J. Ochoa, and T. H. Kinder (1995), The role of the interface in exchange through the Strait of Gibraltar, *J. Geophys. Res.*, *100*, 10,755–10,776.

Curry, R., R. Dickson, and I. Yashayaev (2003), A change in the freshwater balance of the North Atlantic Ocean over the last four decades, *Nature*, *426*, 826–829.

Dietrich, D. E. (1997), Application of a modified "a" grid ocean model having reduced numerical dispersion to the Gulf of Mexico circulation, *Dyn. Atmos. Oceans*, *27*, 201–217.

Dietrich, D. E., B. E. McDonald, and A. Warn-Varnas (1975), Optimized block-implicit relaxation, *J. Comput. Phys.*, *18*, 421–439.

Dietrich, D. E., M. G. Marietta, and P. J. Roache (1987), An ocean modeling system with turbulent boundary layers and topography. Part I: Numerical description, *Int. J. Numer. Methods Fluids*, *7*, 833–855.

Dietrich, D. E., A. Mehra, R. L. Haney, M. J. Bowman, and Y.-H. Tseng (2004a), Dissipation effects in North Atlantic Ocean modeling, *Geophys. Res. Lett.*, *31*, L05302, doi:10.1029/2003GL019015.

Dietrich, D. E., R. L. Haney, V. Fernandez, S. Josey, and J. Tintore (2004b), Air-sea fluxes based on observed annual cycle surface climatology and ocean model internal dynamics: A precise, non-damping zero-phase-lag approach applied to the Mediterranean Sea, *J. Mar. Syst.*, *52*, 145–165.

Drillet, Y., B. Bourdalle-Badie, L. Siefridt, and C. Le Provost (2005), Meddies in the Mercator North Atlantic and Mediterranean Sea eddy-resolving model, *J. Geophys. Res.*, *110*, C03016, doi:10.1029/2003JC002170.

Ezer, T., and G. L. Mellor (2004), A generalized coordinate ocean model and a comparison of the bottom boundary layer dynamics in terrain-following and in z-level grids, *Ocean Modell.*, *6*, 379–403.

Fernandez, V., D. E. Dietrich, R. L. Haney, and J. Tintore (2005), Mesoscale, seasonal and inter-annual variability in the Mediterranean Sea using the DieCAST ocean model, *Prog. Oceanogr.*, *66*, 321–340.

Hellerman, S., and M. Rosenstein (1983), Normal monthly wind stress over the world ocean with error estimates, *J. Phys. Oceanogr.*, *13*, 1093–1104.

Iorga, M. C., and M. S. Lozier (1999), Signatures of the Mediterranean outflow from a North Atlantic climatology: 1. Salinity and density fields, *J. Geophys. Res.*, *104*(C11), 25,985–26,009.

Johnson, R. G. (1997), Climate control requires a dam at the Strait of Gibraltar, *Eos Trans. AGU*, *78*, 277, 280–81.

Johnson, J., I. Ambar, N. Serra, and I. Stevens (2002), Comparative studies of the spreading of Mediterranean water through the Gulf of Cadiz, *Deep Sea Res., Part II*, *49*, 4179–4193.

Killworth, P. (2001), On the rate of descent of overflows, *J. Geophys. Res.*, *106*(C10), 22,267–22,275.

Killworth, P., and N. R. Edwards (1999), A turbulent bottom boundary layer code for use in ocean models, *J. Phys. Oceanogr.*, *29*, 1221–1238.

Lai, C. A. (2006), Effects of gas hydrates on the chemical and physical properties of seawater, *J. Pet. Sci. Eng. Spec. Issue Nat. Gas Hydrate*, *56*, 47–53.

Lai, C. A., D. E. Dietrich, and M. J. Bowman (2005), Global warming and the mining of oceanic methane hydrate, *Top. Catal., Spec. Issue Methane Hydrate Mining*, *32*, 95–99.

Legg, S., R. W. Hallberg, and J. B. Girton (2005), Comparison of entrainment in overflows simulated by z-coordinate, isopycnal and non-hydrostatic models, *Ocean Modell.*, *11*, 69–97, Washington, D.C.

Levitus, S., and T. Boyer (1994), *World Ocean Atlas 1994*, vol. 4, *Temperature*, 150 pp., NOAA Atlas NESDIS 4.

Lozier, M. S., W. B. Owens, and R. Curry (1995), The climatology of the North Atlantic, *Prog. Oceanogr.*, *36*, 1–44.

Maltrud, M. E., and J. L. McClean (2005), An eddy resolving global 1/10 degree ocean simulation, *Ocean Modell.*, *8*, 31–54.

Millot, C. (1999), Circulation in the Western Mediterranean Sea, *J. Mar. Syst.*, *20*, 423–442.

Millot, C. (2007), Interannual salinification of the Mediterranean inflow, *Geophys. Res. Lett.*, *34*, L21609, doi:10.1029/2007GL031179.

Ozkokmen, T., E. P. Chassignet, and C. G. Rooth (2001), On the connection between the Mediterranean outflow and the Azores Current, *J. Phys. Ocean.*, *31*, 461–480.

Pacanowski, R. C., and S. G. H. Philander (1981), Parameterization of vertical mixing in numerical models of tropical oceans, *J. Phys. Oceanogr.*, *30*, 1069–1082.

Peters, H., W. E. Johns, A. S. Bower, and D. M. Frantantoni (2005), Mixing and entrainment in the Red Sea overflow plume. Part II: Plume structure, *J. Phys. Oceanogr.*, *35*, 569–583.

Rixen, M., et al. (2005), The Western Mediterranean Deep Water: A proxy for climate change, *Geophys. Res. Lett.*, *32*, L12608, doi:10.1029/2005GL022702.

Roache, P. J. (1995), *Elliptic Marching Methods and Domain Decomposition*, 190 pp., CRC Press, Inc., Boca Raton, Fla.

Sanderson, B. G., and G. Brassington (1998), Accuracy in the context of a control-volume model, *Atmos. Ocean*, *36*, 355–384.

Smith, R. D., M. E. Maltrud, F. D. Bryan, and M. M. W. Hecht (2000), Numerical simulation of the North Atlantic Ocean at 1/10°, *J. Phys. Oceanogr.*, *30*, 1532–1561.

Staneva, J., D. Dietrich, E. Stanev, and M. Bowman (2001), Rim current and coastal eddy mechanisms in an eddy-resolving Black Sea general circulation model, *J. Mar. Syst., Spec. Issue Black Sea*, *31*, 137–157.

Teague, W. J., M. J. Carron, and P. J. Hogan (1990), A comparison between the Generalized Digital Environmental Model and Levitus climatologies, *J. Geophys. Res.*, *95*, 7167–7183.

Tintore, J., P. E. La Violette, I. Blade, and A. Cruzado (1988), A study of an intense density front in the eastern Alboran Sea: The Almeria-Oran front, *J. Phys. Oceanogr.*, *18*, 1384–1397.

Tseng, Y.-H., and L. C. Breaker (2007), Nonhydrostatic simulations of the regional circulation in the Monterey Bay area, *J. Geophys. Res.*, *112*, C12017, doi:10.1029/2007JC004093.

Tseng, Y.-H., and D. E. Dietrich (2006), Entrainment and transport in idealized three-dimensional gravity current simulation, *J. Atmos. Ocean. Technol.*, *23*, 1249–1269.

Tseng, Y.-H., and J. H. Ferziger (2001), Mixing and available potential energy in stratified flows, *Phys. Fluids*, *13*, 1281–1293.

Tseng, Y.-H., J. H. Ferziger, and D. E. Dietrich (2005), Regional circulation of the Monterey Bay region-hydrostatic versus non-hydrostatic modeling, *J. Geophys. Res.*, *110*, C09015, doi:10.1029/2003JC002153.

Viudez, A., J. M. Pinot, and R. L. Haney (1998), On the upper layer circulation in the Alboran Sea, *J. Geophys. Res.*, *103*, 21,653–21,666.

Willebrand, J., B. Barnier, C. W. Boning, C. Dietrich, P. O. Killworth, C. LeProvost, Y. Jia, J. M. Molines, and A. L. New (2001), Circulation characteristics in three eddy-permitting models of the North Atlantic, *Prog. Oceanogr.*, *48*, 123–161.

M. J. Bowman, Marine Sciences Research Center, State University of New York at Stony Brook, Stony Brook, 215 Endeavour Hall, NY, USA.

D. E. Dietrich, AcuSea, Inc., 8450-101 Via Sonoma, La Jolla, CA, USA.

M. Liste, R. Medina, and M. Olabarrieta, Ocean and Coastal Research Group, University of Cantabria, 39005 Av. Castros, Santander, Spain.

A. Mehra, Environmental Modeling Center, NCEP/NWS, NOAA, 5200 Auth Road, Camp Springs, MD, USA.

S. A. Piacsek, Oceanography Division, Naval Research Laboratory, Stennis Space Center, 1002 Balch Blvd., MS, USA.

Y.-H. Tseng, Department of Atmospheric Sciences, National Taiwan University, No. 1, Sec. 4 Roosevelt Road, Taipei 10617 Taiwan. (yhtseng@webmail.as.ntu.edu.tw)